



# Size effects of voids on the mechanical properties of 3D printed parts

Hassan Gonabadi<sup>1</sup> · Seyed Farhad Hosseini<sup>2</sup> · Yao Chen<sup>1</sup> · Steve Bull<sup>1</sup>

Received: 30 December 2023 / Accepted: 23 April 2024 / Published online: 2 May 2024  
© The Author(s) 2024

## Abstract

Although the effects of additive manufacturing process parameters on the mechanical properties of 3D printed parts have been numerically investigated in the literature, less attention has been paid on the size effects of voids between deposited filaments. This study fills this gap by developing a methodology based on a combined finite element (FE) and design of experiment (DoE) technique. The development of FE methodology is based on micro-mechanical analysis of representative volume element (RVE) of 3D printed parts to predict the effective orthotropic properties. To account for the size effects of inter-bead voids, the RVE includes contribution of the multiple parameters of layer heights, layer widths and overlapping regions. To study the main and interaction effects of the above input parameters on the stiffness properties of 3D printed parts, a structured approach based on full factorial design is used. Although the size effects of voids on the constituents of elastic moduli of RVE were investigated, the main focus in the present work is to develop a regression model to predict the stiffness properties. The FE stress analysis of the RVE conducted in this study provides an insight about the potential failure modes such as delamination and filament debonding that may occur in load bearing 3D printed parts. For a case study, the results of FE-based homogenization technique in terms of stiffness properties are validated against the experimental data via three-point bending and Iosipescu shear tests which were conducted in conjunction with digital image correlation technique. The combined numerical and statistical approach proposed in this study provides a swift iterative design of 3D printed parts prior to the time-consuming computation modelling, contributing to reduce the number of tests and manufacturing costs.

**Keywords** 3D printed parts · Design of experiment · Finite element homogenization · Micro-mechanical analysis · Representative volume element

## 1 Introduction

In recent years, significant advancements in additive manufacturing (AM) technology have revolutionized the production of lightweight components featuring intricate geometries. This progress has had a profound impact across various sectors including automotive, aerospace, military, marine, biomedical, and electronics industries. Among the array of lightweight parts, 3D printed components hold a distinct significance due to their ability to achieve requisite mechanical properties through tailored microstructures.

Within additive manufacturing (AM), fused filament fabrication (FFF) stands out as a well-established method for rapid prototyping, enabling the fabrication of lightweight parts with intricate 3D geometries. This process involves the gradual buildup of an extruded filament, typically a thermoplastic material, through a layer-by-layer deposition process. In this process, the filament is guided through a heated nozzle, where it reaches a semi-molten state before being precisely applied to the build platform. It is crucial to maintain optimal feed rates during 3D printing to prevent premature solidification of each layer before the subsequent layer can be added, ensuring proper bonding between layers.

Common thermoplastic filament materials utilized in FFF 3D printers, processed through heated nozzles, include acrylonitrile butadiene styrene (ABS), polylactic acid (PLA), nylon, polypropylene (PP), and polyethylene terephthalate (PET). Throughout the FFF 3D printing process, each filament, upon extrusion through the heated nozzle, undergoes solidification, facilitating the formation of bonds between

---

✉ Hassan Gonabadi  
Hassan.gonabadi57@gmail.com

<sup>1</sup> School of Engineering, Newcastle University,  
Newcastle upon Tyne NE1 7RU, UK

<sup>2</sup> Hamburg University of Technology, Am  
Schwarzenberg-Campus 4 (C), 21073 Hamburg, Germany

adjacent deposited filaments. Consequently, polymer sintering engenders the creation of bridges (necks) between the deposited filaments.

The mechanical behaviour of FFF 3D printed parts is different compared with parts manufactured by conventional method (e.g., injection moulding). This is mainly due to the existence of voids and gaps between the deposited filaments which reduces the layer-to-layer bond strength, and as a result, the mechanical properties of FFF 3D printed components are compromised by voids which develop localized stresses at the bond between two deposited filaments. This leads to a deformation between layers (inter-layer) and within layers (intra-layer) in the form of cracks, delamination or even failure.

Among different classifications of voids such as raster gap, partial neck growth, sub-perimeter, intra-bead and infill voids [1], partial neck growth voids (i.e., inter-bead voids) are basically formed because of the incomplete neck growth between adjacent deposited filaments [2], which is mainly due the mechanism of viscous sintering. Although, in the ideal condition of 100% diffusion of two raster layers at the interface during solidification, this type of void formation could be avoided, realistic conditions during the FFF 3D printing are incapable of sustaining neck development beyond a short-term period of time (i.e., a few seconds) after material deposition [3], meaning that the raster are solidified before completing coalescence [4, 5]. As a result, partial neck growth voids known as inter-bead voids formed between raster and layers are unavoidably wiped out completely due to certain inherent characteristics of the FFF 3D printing, such as incomplete filling and inconsistent material flow [6]. Although the formation of inter-bead voids as a 3D structural element makes a positive contribution to reduce the weight and improve the functionality, in load bearing components which require optimal mechanical performance, the existence of inter-bead voids is undesirable.

Several studies have investigated the effect of voids on the mechanical properties of 3D printed parts. Tronvoll et al. used a statistical approach to quantify the impact of voids on the mechanical properties of 3D printed parts, indicating that void size significantly influences strength and contributes to anisotropic behaviour in FDM specimens [7]. Wang et al. investigated the impact of microscopic voids on the mechanical properties of materials fabricated through FDM by combining experiments and micro-mechanical modelling, utilizing X-ray computed tomography (XCT) to characterize the voids and also to propose a model to predict mechanical properties based on porosity, resulting in a cost-saving tool for designers to predict elastic properties of 3D printed materials [8]. In a different study, He et al. investigated the adverse effects of microscopic voids on the mechanical properties of 3D printed continuous carbon fibre-reinforced polymer composites, emphasizing the importance of minimizing void content

during the 3D printing process to enhance performance and expand practical applications [9]. Sayah and Smith studied the void characteristics within the microstructure of short carbon fibre-reinforced acrylonitrile butadiene styrene (SCF/ABS) composites produced via additive manufacturing, finding that void volume fraction varies across different 3D printing methods and process parameters, with deposition on the print bed and the use of a roller during printing leading to reduced void volume fraction [10]. In a different study, the influence of process parameters on dimensional accuracy, void content and mechanical properties of 3D printed short carbon fibre-reinforced composites has been investigated to predict void sizes and their effects on mechanical properties, ultimately optimizing parameters to minimize dimensional variability and void content while maximizing structural performance [11]. Chung et al. investigated the impact of anisotropic voids, generated via 3D printing, on the properties of insulating media, showing that strategically arranged anisotropic voids can significantly reduce thermal conductivity while affecting mechanical strength, suggesting potential for developing high-performance insulating materials with tailored void sizes [12].

Although the mechanisms of void formation in FFF 3D printed parts for all the classifications of voids as described earlier depend on the 3D printing process parameters, the existence of inter-bead voids can be controlled by three important variables of layer height, layer width and the amount of overlap between adjacent deposited filaments: all these variables can be set by the manufacturers and designers before the process of 3D printing the final product is started.

Although the experimental approach can be used to investigate the size effects of inter-bead voids on the mechanical properties of parts, a huge number of experimental repeats and therefore high costs are required to avoid uncertainty and materials variability. One way to avoid these experimental repeats and their associated cost/time is the use of numerical methods (i.e., computational modelling) to predict the effect of these parameters/size effects of voids on the mechanical properties, although this method is also limited mainly due to the increased number of elements required for meshing the complex 3D printed parts, making this method computationally expensive. To address this, micromechanics-based analysis of a repeating unit cell has been developed [6, 13–15], resulting in the derivation of analytical expressions as well as numerical methods for the structure-property relationships. FE-based homogenization techniques to predict the mechanical response of 3D printed and composite structures have been investigated previously in the literature [16–22], and the results show that FE modelling of representative volume elements (RVE) is an option when it comes to the analysis of such parts with regular repeating unit cells. Hedayati et al. employed analytical, numerical and experimental methods to investigate the mechanical properties of additively manufactured biomaterials, revealing close agreement between finite

element-based homogenization techniques and experimental results, highlighting the significance of considering directional effects for predicting the mechanical response of 3D printed and composite structures [17]. The method outlined in this study [18] established a rigorous foundation in mechanics, utilizing finite element analysis on representative volume elements to accurately predict the mechanical properties of 3D printed and composite structures, emphasizing the necessity of correct boundary conditions and leveraging symmetry and periodicity considerations to relate non-homogeneous stress and strain fields within the RVEs to average values and ultimately yielding results consistent with theoretical predictions and experimental data. Tucker et al. evaluated the micro-mechanics models, including the dilute model based on Eshelby's equivalent inclusion, self-consistent model, Mori-Tanaka models, bounding models, Halpin-Tsai equation and shear lag models, in the context of finite element-based homogenization techniques for predicting the mechanical response of 3D printed and composite structures, finding that the Mori-Tanaka model and the bound interpolation model provide the most accurate predictions when compared to finite element calculations and boundary element results [19]. In a different study, the Voronoi/Monte Carlo technique was coupled with Voronoi and Monte Carlo algorithms to generate two-dimensional random cellular structures, allowing for the simulation of various structural effects such as cell density, elongation, local concentration, gradient and defects, which are then analyzed using finite element-based homogenization techniques to predict the mechanical response of 3D printed and composite structures [20]. Liu and Shapiro proposed two-stage approach utilizing finite element-based homogenization techniques to predict the mechanical response of 3D printed and composite structures by constructing an effective meso-scale geometry-material model of the printed structure and homogenizing it at the macro-scale through solving an integral equation formulated using Green's function [21]. Finally, Park et al. proposed a two-step homogenization method within finite element analysis to predict the mechanical behaviour of 3D printed structures, considering the additive manufacturing process intricacies and employing unit cell discretization for effective property estimation and validation against experimental results [22].

In the FE homogenization technique, the calculation of macro-scale mechanical properties of materials is based on the properties of thermoplastic materials used for 3D printing (i.e., filament) and geometrical microstructure of the unit cell. In this technique, the 3D printed part is considered a continuum, and a small volume element of a periodic unit cell known as an RVE is considered for numerical homogenization. Experimental characterization via a wide range of standard mechanical testing has been carried out to obtain the orthotropic elastic constants of FFF printed samples, and the results have been compared with FE simulation showing

good agreement between model predictions and experimental data [23, 24]. In different works, a two-step homogenization approach is used for the analysis of 3D printed structures with more complex design, based on the estimation of homogenized stiffness properties of RVE and then using these properties for the subsequent mechanical simulation of global elastic response [25, 26].

In the present study, the RVE of FFF-based 3D printed parts with different layer heights, layer widths and overlaps were developed using computer aided design tool to determine the size effects of inter-bead voids on the effective orthotropic engineering constants. This is done by FE analysis of RVEs using micro-mechanics plug-in in the FE software ANSYS (Material Designer). Although the effects of layer height on the elastic response of 3D printed parts have been experimentally investigated in the literature [27, 28], the present study focuses on the FE analysis technique, providing more reliability and certainty. In addition, capturing the effects of overlaps and layer width on the mechanical properties of 3D printed parts using methodologies developed in the present work is a previously unexplored research area. In order to determine the relationship between the above variables of layer height, layer width and overlapping (i.e., size effects of voids) and stiffness properties of RVE, a structured methodology based on design of experiment was used giving insights about the main effects as well as the interaction effects of the above input parameters on the stiffness constituents as well as the stress concentration of 3D printed parts. In addition, using the methodology of DoE, it is possible to conduct the regression fitting analysis and to predict the stiffness properties of 3D printed parts especially at the levels of factors which are not included in the DoE. Finally, the size effects of voids on the constituents of elastic modulus of RVE are investigated. The combined methodology of FEA and DoE proposed in the present work facilitates setting the 3D printing process parameters by designers for a given set of materials, boundary conditions and constraints to manufacture FFF-based 3D printed parts and structures with optimized mechanical behaviour, eventually contributing to reducing the number of tests and manufacturing costs before industrial application.

## 2 Methodology

The current research focuses on developing representative volume elements (RVEs) for fused filament fabrication (FFF)-based 3D printed components, varying parameters such as layer heights, layer widths and overlaps. A geometric modeller via ANSYS workbench tool is employed to define the shape of the domain. By parametrizing the model geometry according to these variables, the study investigates the impact of inter-bead voids on the effective orthotropic engineering constants.

This is achieved through finite element (FE) simulation of RVEs using micro-mechanics plug-in in ANSYS software (Material Designer). While previous studies have explored the influence of layer height on the elastic response of 3D printed parts experimentally, this research emphasizes the FE analysis technique, offering greater reliability. Additionally, the study delves into the effects of overlaps and layer width on the mechanical properties of 3D printed parts, an area not extensively researched before. A structured methodology based on design of experiment is utilized to determine the relationship between layer height, layer width, overlapping of RVEs and stiffness properties, revealing both main effects and interaction effects of these parameters. Finally, the study examines the size effects of voids on the elastic modulus of RVE constituents.

It is important to acknowledge that for this study, certain factors, such as printing speed and printing temperature, were intentionally excluded from the design of experiment (DoE) for several specific reasons:

- The primary objective of this study was to delve into specific process parameters. Due to constraints such as time, resources and the intricacy of incorporating additional variables, printing speed and temperature were omitted from the DoE. By narrowing the focus of our investigation, we could delve deeper into the effects of the selected parameters, namely layer height, layer width and overlapping regions. This approach allowed us to provide more comprehensive insights within the confines of our study limitations.
- While acknowledging the significance of printing speed and printing temperature as critical parameters, it is essential to note that these factors have been extensively examined in prior experimental research. In our current study, we aimed to contribute novel insights by exploring less-explored variables such as layer height, layer width and overlap, while also examining interactions between these parameters.
- A crucial aspect of our experimental design was to meticulously control variables and isolate the effects of the chosen parameters. Incorporating additional factors like printing speed and temperature could have introduced heightened complexity and confounding variables, potentially obscuring the clarity of our results.
- Furthermore, conducting numerical analysis using finite element analysis (FEA) in this study involving printing speed and temperature necessitated specific interfaces between different modules in FE software. Unfortunately, such interfaces have not yet been programmed into the current commercial FE software. Therefore, given our resource limitations, we prioritized other aspects of the study. However, we recognize that in our future research, utilizing an experimental approach rather than a numerical method, we could thoroughly explore the parameters of printing speed and printing temperature.

**Table 1** Variables and levels used in the DoE

Factors	Levels		
	1	2	3
Layer height (mm)	0.12	0.2	0.28
Layer width (mm)	0.15	0.25	0.35
Overlap region (%)	1	5	10

## 2.1 Design of experiment

The main objective of this study is to investigate the void size effects on the mechanical properties of 3D printed parts; therefore, to set up the design of experiment, layer height, layer width and overlap region were selected as the most important variables due to their significant effects on the inter-bead void size. The elastic constants of RVE of FFF-based 3D printed parts, i.e., three Young's moduli of  $E_1$ ,  $E_2$  and  $E_3$  and three shear moduli  $G_{12}$ ,  $G_{23}$  and  $G_{13}$ , were selected as the response. The variable parameters along with their levels are shown in Table 1. It must be noted that apart from the above variable parameters, other factors such as temperature of deposition are also important as they control the polymer viscosity and bond penetration of one filament to another; however, in this study, this factor has been already considered by considering different overlapping regions between adjacent deposited filaments, and therefore, this factor was constrained in this study. In addition, infill pattern and build orientation in 3D printed parts are another variables affecting the void size and mechanical properties; however, for the sake of consistency, only one infill pattern of grid with the layers of filaments laid up at  $0^\circ$  and  $90^\circ$  and the build orientation of  $0^\circ$  flat has been taken into consideration in this study, and therefore, these factors were also constrained in the programme for DoE. The full factorial design of experiment with three factors as the main variable parameters, each at three levels, given in Table 1, was used to investigate the effects of each of the factors on the elastic constants. This is to screen out the most important from the less important effects. With the full factorial design of experiments, a total number of 27 runs are given as the design matrix in Table 2.

## 2.2 Micro-mechanical analysis of RVE based on FE homogenization method

The method of prediction of the constitutive matrix (i.e., effective orthotropic properties) based on the isotropic properties of constituent materials, geometrical aspects of the microstructure and the inter-bead voids inherited from the 3D printing strategy is called homogenization. Figure 1 shows a schematic illustration of 3D FFF printer where the model is built layer by layer. With reference to this figure, the overlapping region in 3D printed

**Table 2** Design matrix of DoE

Std-order	Run-order	Layer height (mm)	Layer width (mm)	Overlap (%)
25	1	0.28	0.35	1
27	2	0.28	0.35	10
5	3	0.12	0.25	5
26	4	0.28	0.35	5
14	5	0.2	0.25	5
13	6	0.2	0.25	1
16	7	0.2	0.35	1
24	8	0.28	0.25	10
9	9	0.12	0.35	10
22	10	0.28	0.25	1
7	11	0.12	0.35	1
15	12	0.2	0.25	10
6	13	0.12	0.25	10
12	14	0.2	0.15	10
19	15	0.28	0.15	1
21	16	0.28	0.15	10
18	17	0.2	0.35	10
20	18	0.28	0.15	5
17	19	0.2	0.35	5
23	20	0.28	0.25	5
11	21	0.2	0.15	5
2	22	0.12	0.15	5
1	23	0.12	0.15	1
8	24	0.12	0.35	5
3	25	0.12	0.15	10
10	26	0.2	0.15	1
4	27	0.12	0.25	1

FFF-based part refers to the area where adjacent printed layers intersect or partially overlap during the printing process. When each layer of filament is deposited, it

slightly overlaps with the previous layer. This overlapping ensures proper adhesion between layers and improves the structural integrity of the printed part. The overlapping region serves as a bonding interface between adjacent filaments, contributing to the overall strength and stability of the final printed object. It must be noted that in Fig. 1, the layer width refers to the horizontal width of the extruded filament (i.e., width of the bead) as it is deposited by the printer’s nozzle during each layer of the printing process. It determines the width of each printed line or trace that forms the individual layers of the printed object. As shown in Fig. 2, the RVE is considered from a layer of printed part, and it is treated as macroscopically homogeneous orthotropic material. In the 3D printing technique, the effective orthotropic properties are calculated from the properties of the filament raw materials used for printing, where in this study, two normalized elastic constants of Young’s modulus and Shear’s modulus were used. For each trial in the design matrix as shown in Table 2, micro-mechanical models of RVE based on the layer height, layer width and the amount of overlap were developed in the design modeller tool of ANSYS workbench. To generate meshing, four-node tetrahedral elements were used for the micro-models of the RVEs, then these RVEs are loaded to six different states of tensile and shear strains applied individually using the periodic boundary condition [29, 30]. It must be noted that in this study, utilizing the material symmetry along the 13 plane, half of the RVE model as shown in Fig. 2 was effectively modelled, significantly reducing computational costs in the FE analysis while maintaining accurate representation of the entire structure’s behaviour. FE analysis of the micro-models of RVEs was carried out using the micro-mechanics plug-in in ANSYS (Material Designer) resulting in effective orthotropic properties. For the computational homogenization analysis of RVEs,

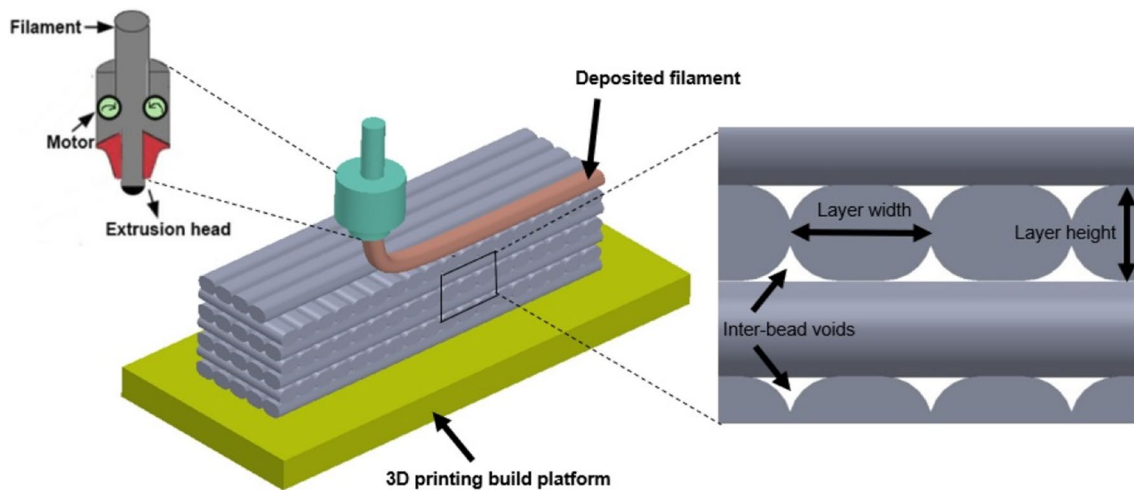


**Fig. 1** Schematic view of 3D fused filament fabrication (FFF) printer where the model is built layer by layer

Fig. 2 RVE of 3D printed part

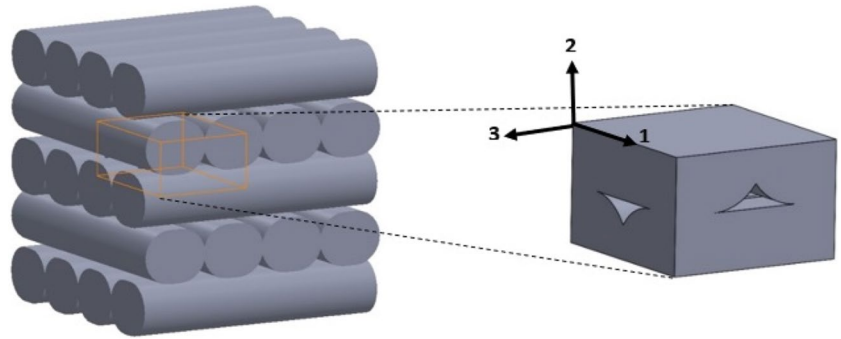
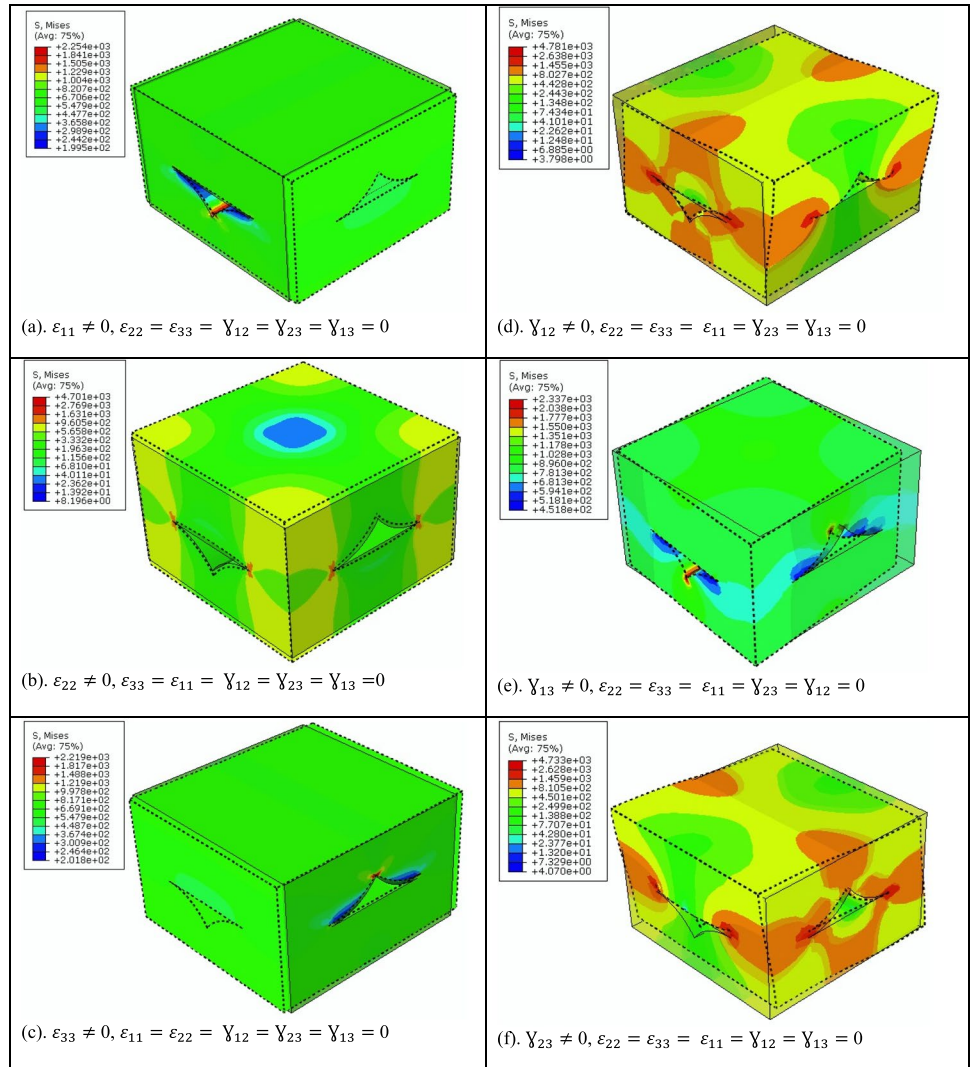


Fig. 3 Stress fields of the RVE of 3D printed part subjected to six states of uniaxial and shear strains. The deformed and un-deformed shapes of RVE are shown in dashed and solid lines, respectively



convergence of the simulation results is verified, and the mesh dependency is avoided by using smaller elements. It must be noted that in this study, in the FE homogenization modelling technique, only the elastic response of 3D printed parts was simulated, and viscoelastic and/or plastic behaviour of filament materials were not taken into consideration.

### 3 Results and discussions

#### 3.1 FE analysis of RVE

Figure 3 shows the stress distribution of the RVE when loaded to six states of uniaxial and shear strains. By applying longitudinal tensile, transverse tensile and

**Fig. 4** Multi-scale FE-based homogenization analysis executed to map the strain distribution of 3D printed specimen under 3 PB and Iosipescu shear tests. (a) Micro-scale of RVE with the layer height of 0.2 mm, layer width of 0.3 and overlap of 3%; (b) RVE at meso-scale level; and (c) macro-scale model of three-point bending test and Iosipescu shear coupons

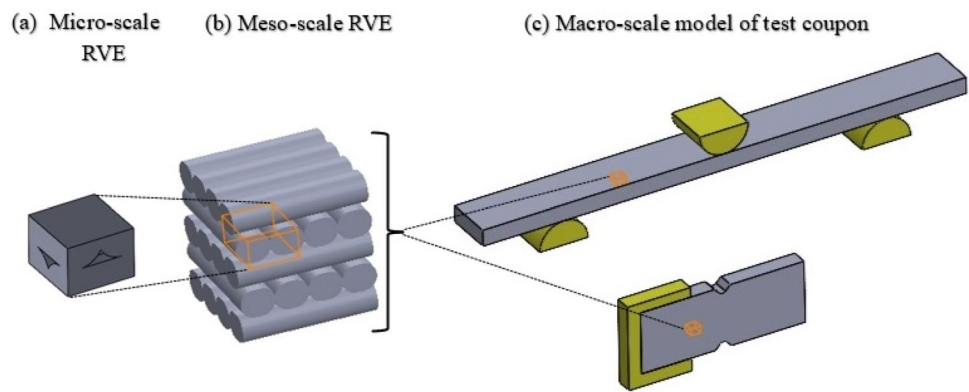


**Table 3** FE-computed effective orthotropic properties of RVE of SCF/PA composite at both micro-scale and meso-scale levels

Properties	Micro-scale RVE
Longitudinal elastic modulus $E_1$ (GPa)	2.84
Out-of-plane modulus $E_2$ (GPa)	0.95
In-plane transverse modulus $E_3$ (GPa)	2.84
Major Poisson's ratio ( $\nu_{12}$ )	0.34
Minor Poisson's ratio ( $\nu_{13}$ )	0.31
Minor Poisson's ratio ( $\nu_{23}$ )	0.11
Inter-laminar shear modulus $G_{12}$ (GPa)	0.53
Inter-laminar shear modulus $G_{23}$ (GPa)	0.53
In-plane shear modulus $G_{13}$ (GPa)	1.05

in-plane shear load cases (i.e.,  $\epsilon_{11}$ ,  $\epsilon_{22}$  and  $\gamma_{13}$ ), maximum localized stresses (i.e., stress hot spots) are observed at the intersection of the adjacent deposited filaments in the overlapping regions. This is obviously because there is less material across the section and also due to the specific geometric feature of the RVE. Therefore, the weakest area in the microstructure is the intersection of the deposited filaments, and it is susceptible to crack initiation and debonding between the deposited filaments during the mechanical loading. In addition, by applying through the thickness and inter-laminar shear load cases (i.e.,  $\epsilon_{22}$ ,  $\gamma_{12}$  and  $\gamma_{23}$ ), the highest localized stresses compare to other load cases are observed. Such loading can finally induce delamination between layers, leading to the failure of the 3D print parts.

### 3.2 Validation of FE-calculated stiffness properties of RVE

It has been shown in previous study that by providing an accurate characterization of the properties to be fed into the macro-scale model, the use of the homogenization technique is a reliable tool to predict the elastic response of 3D printed parts [24]; as a result, in the present study,

the results of FEA are validated against the experimental data via the mechanical testing programme of three-point bending (3 PB) and Iosipescu shear tests. To simulate the 3 PB and shear tests, a multi-scale FE homogenization framework is used (Fig. 4). Initially, a set of values for layer height, layer width and overlap (e.g., 0.2 mm, 0.3 mm and 3% respectively), which were not included in the current design matrix, was used to generate the RVE. By conducting micro-mechanical analysis using an FE-based homogenization technique on this newly developed RVE, FE-computed effective orthotropic properties are calculated (Table 3), and then the results were used as an input for the creation of a macro-scale FE modelling and simulation of 3 PB and Iosipescu shear tests resulting in the strain field maps which can then be validated against the experimental data.

#### 3.2.1 Sample preparation and mechanical tests

The 3 PB and Iosipescu shear test specimens were produced using a FFF 3D printer (Ultimaker 3), and then mechanical testing in conjunction with digital image correlation (DIC) was carried out to obtain the full field strain maps. A polylactic acid (PLA) filament provided by Ultimaker (standard silver metallic PLA, 2.85 mm/750 g) was used to obtain the 3D printed specimens. The Ultimaker Cura 4.8 edition was used to generate the machine code for the FFF 3D printer from the 3D model files. The 3D printing process parameters used to produce the test specimens are provided in Table 4. The 3 PB and Iosipescu test specimens were 3D printed with different raster and build orientations using deposited filaments laid at ( $0^\circ$ ,  $90^\circ$ ). The summary of printing patterns and orientation for different types of test specimens are shown in Fig. 5. It must be noted that in the conventional additive manufacturing process, it is customary to produce a shell of maximum density covering the entire surface of the object, with the remaining volume filled using a cross-layered raster structure. However, in this study, we intentionally omitted the use of a shell

**Table 4** 3D printing process parameters used to produce the 3 PB test coupons

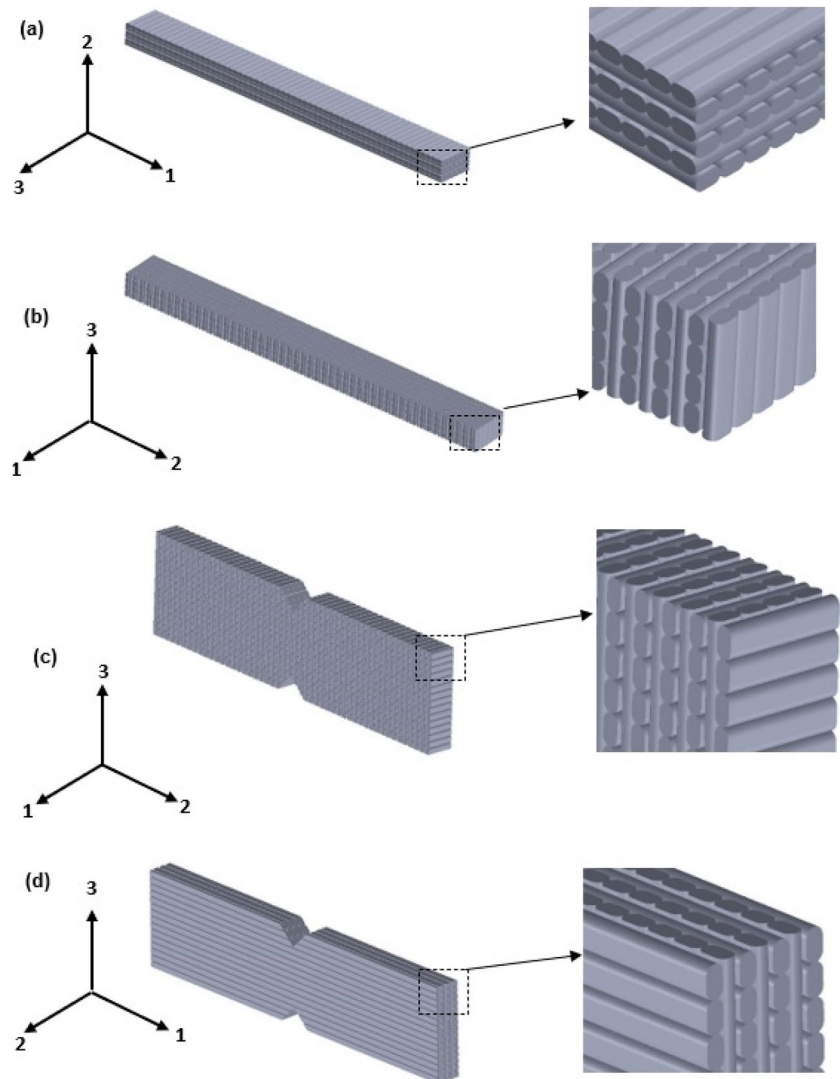
Parameter	Description
Extrusion temperature (°C)	250
Flow multiplier (%)	100
Deposition speed (mm/s)	60
Bed temperature (°C)	110
Nozzle diameter (mm)	0.4
Layer thickness (mm)	0.2
Strand overlap (%)	3
Infill pattern of grid	Filament layout at (0°,90°)
Infill density	100%
Layer width (mm)	0.3
Material of the build platform	Glass platform

layer. Consequently, the test specimens were printed solely using the cross-layered raster structure. In addition, since the longitudinal modulus and transverse modulus ( $E_1 = E_3$ )

are equivalent, to prevent redundancy, the schematic view of the 3D printed flexural test specimen, which facilitates the calculation of the transverse modulus ( $E_3$ ), is omitted from Fig. 5. Moreover, as  $G_{12}$  and  $G_{23}$  are identical, the schematic view of the 3D printed Iosipescu test specimen, which aids in determining the shear modulus ( $G_{12}$ ), is also excluded from Fig. 5.

To generate the experimental data, 3D printed test specimens were subjected to a 3 PB and shear test in conjunction with DIC system to map the strain fields. It should be noted that in this investigation, instead of employing the circular cross-section of filaments to replicate the bonding induced by nozzle compression between filaments and layers, a rounded rectangular cross-section is utilized with a slight overlap between adjacent filaments. The shape of individual filaments and the overlapping region within the 3D printed sample, as observed under a microscope, are depicted in Fig. 6. Utilizing a calibrated light microscope, the filament's height and width

**Fig. 5** Schematic representation of 3D printed flexural and Iosipescu shear test specimens which 3D printed at different raster angle and build orientation. 3D printed flexural test specimens with **a** raster angle of 0°, **b** build orientation of upright, **c** 3D printed Iosipescu shear test specimen with the build orientation of upright and **d** 3D printed Iosipescu shear test specimen with raster angle of 0°



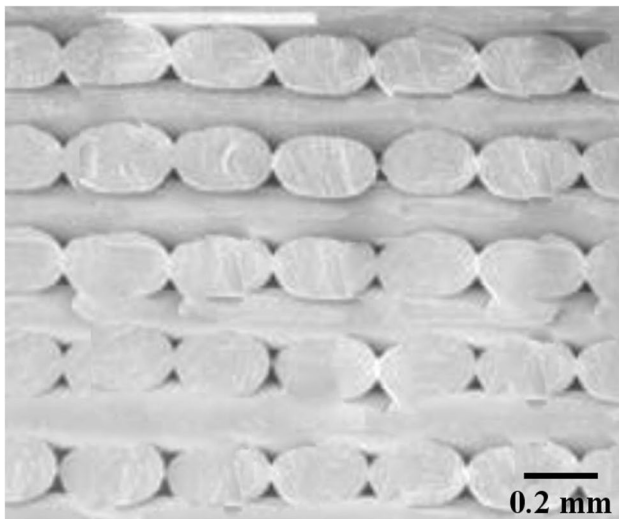


**Fig. 6** A microscopic image displaying the cross-section of raster layers from a 3D printed specimen illustrates the geometric dimensions of deposited filaments, including their width and height

are determined to be 0.2 mm and 0.3 mm, respectively. These measurements were in fact employed to reconstruct a more realistic geometric model of the meso-scale RVE for FE modelling, as illustrated in Fig. 4 (a and b).

### 3.2.2 Macro-scale FE modelling of 3D printed test samples

The macro-scale FE model characterizes the design of 3 PB and Iosipescu shear test specimens using orthotropic properties of RVE with the layer height of 0.2 mm, layer width of 0.3 mm and overlapping region of 3% which are detailed in Table 3. The FE model incorporates the boundary conditions with the internal lay-up of the RVE. In the first stage of FE modelling of the 3 PB and Iosipescu test specimens, a design modelling tool is used to create a shell model of the test specimen. The model integrates the geometry of test specimens according to the standard methods detailed in [24]. The surface function is used to generate a thin surface, then it is transferred into the ANSYS Composite Processor (ACP) where effective engineering constants of the RVE (Table 3) are defined. In the FE mesh sensitivity study, boundary conditions imposed on the FE model of 3 PB and Iosipescu shear test coupons and the contact type between support/loading rollers are all detailed in previous work [24]. It must be noted that in order to provide input data (i.e., orthotropic engineering constants of the RVE) for the FE model of 3D printed sample, FE analysis of RVE with the isotropic properties of PLA filament, (i.e.,  $E = 3500$  MPa and  $\nu = 0.35$ ) was conducted using the homogenization method. Figure 7 shows that the FE- and

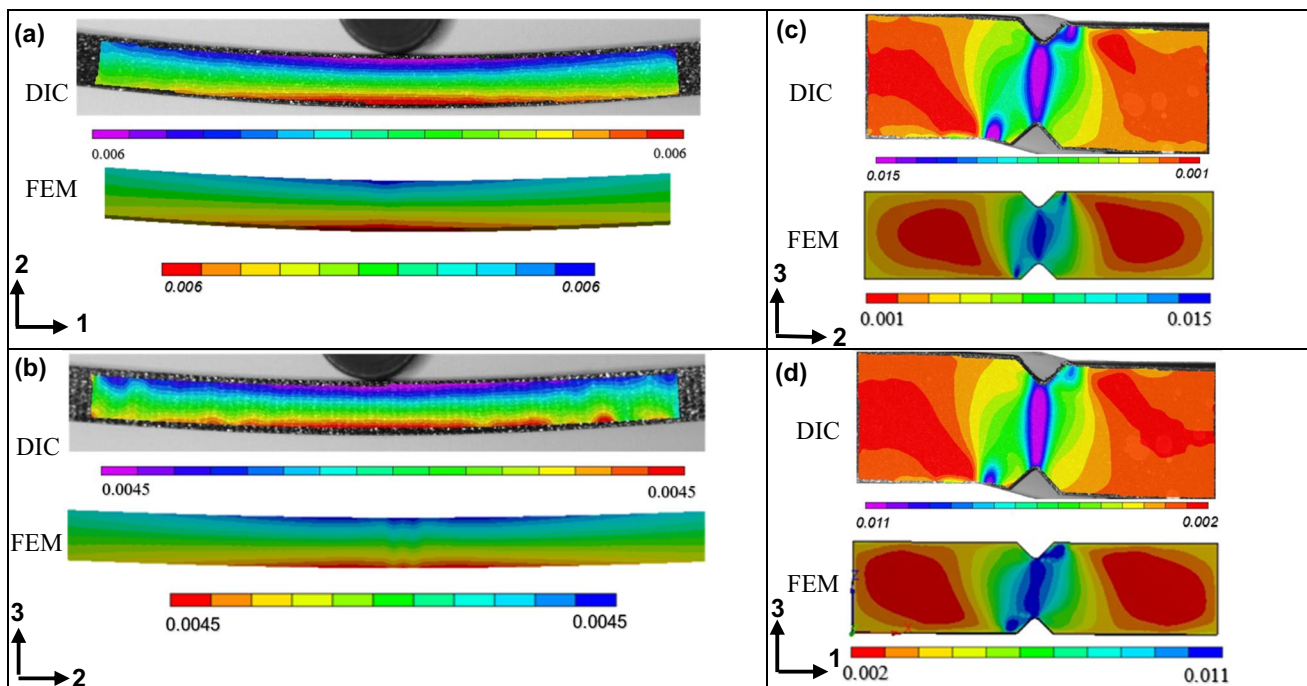


**Fig. 7** DIC versus FE-calculated strain maps of 3D printed 3 PB and Iosipescu test specimens which are printed at different raster angle and build orientation. 3D printed flexural test specimens with **a** raster angle of  $0^\circ$  at the load ( $F_{exp.} = 40.5$  N and  $F_{FEA} = 42.6$  N) and displacement of 2 mm, **b** 3D printed flexural test specimens with build orientation of upright at the load ( $F_{exp.} = 9.6$  N and  $F_{FEA} = 10.7$  N)

and displacement of 1.5 mm, **c** 3D printed Iosipescu shear test specimen with the build orientation of upright at the load of ( $F_{exp.} = 455$  N and  $F_{FEA} = 500$  N) at the stress value of 8 MPa and **d** 3D printed Iosipescu shear test specimen with raster angle of  $0^\circ$  at the load of ( $F_{exp.} = 680$  N and  $F_{FEA} = 750$  N) at the stress value of 12 MPa

DIC-calculated strain fields in different type of 3 PB and Iosipescu shear tests are in close agreement.

### 3.3 Influence of layer height, layer width and overlapping on the effective orthotropic properties of RVE

The main objective of this study is to investigate the size effects of voids on the mechanical properties of 3D printed parts. Among different 3D printing process parameters affecting the size of inter-bead void within the RVE of FFF-based 3D printed parts, layer height, layer width and overlapping are considered in this study. Therefore, initially, the main and interaction effects of these 3D printing variables on the components of elastic modulus of RVE were evaluated. It must be noted that due to the infill pattern of grid, FE analysis of RVE shows that the longitudinal elastic modulus ( $E_1$ ) is the same as transverse modulus ( $E_3$ ) and also inter-laminar shear modulus in plane 1–2 ( $G_{12}$ ) is the same as inter-laminar shear modulus in plane 2–3 ( $G_{23}$ ).

Figure 8 shows the main effects of these variables on the elastic constituents. As it can be seen in these figures, although all parameters of layer height, layer width and overlap have a significant impact on the elastic constituents of RVE, the effect of overlap on the through-thickness and inter-laminar shear properties is less significant compared to the effect of layer height and layer width. The graphs also indicate that although increasing layer width and overlap improves the stiffness properties of RVE, increasing the layer height has a negative impact on the stiffness properties.

Analysis of interaction effects of these variables on the stiffness properties of RVE as shown in Fig. 9 indicates that although the interaction effects are not strong when it comes to the in-plane stiffness properties of the RVE ( $E_1$ ,  $E_3$  and  $G_{13}$ ), interaction effect between layer height and the layer width is tangible and affects the through-thickness and inter-laminar shear properties of the RVE ( $E_2$ ,  $G_{23}$  and  $G_{12}$ ) even more significantly than the main effect of overlapping. The interaction only exists between the layer height and layer width and the interactions effect of layer width/overlapping

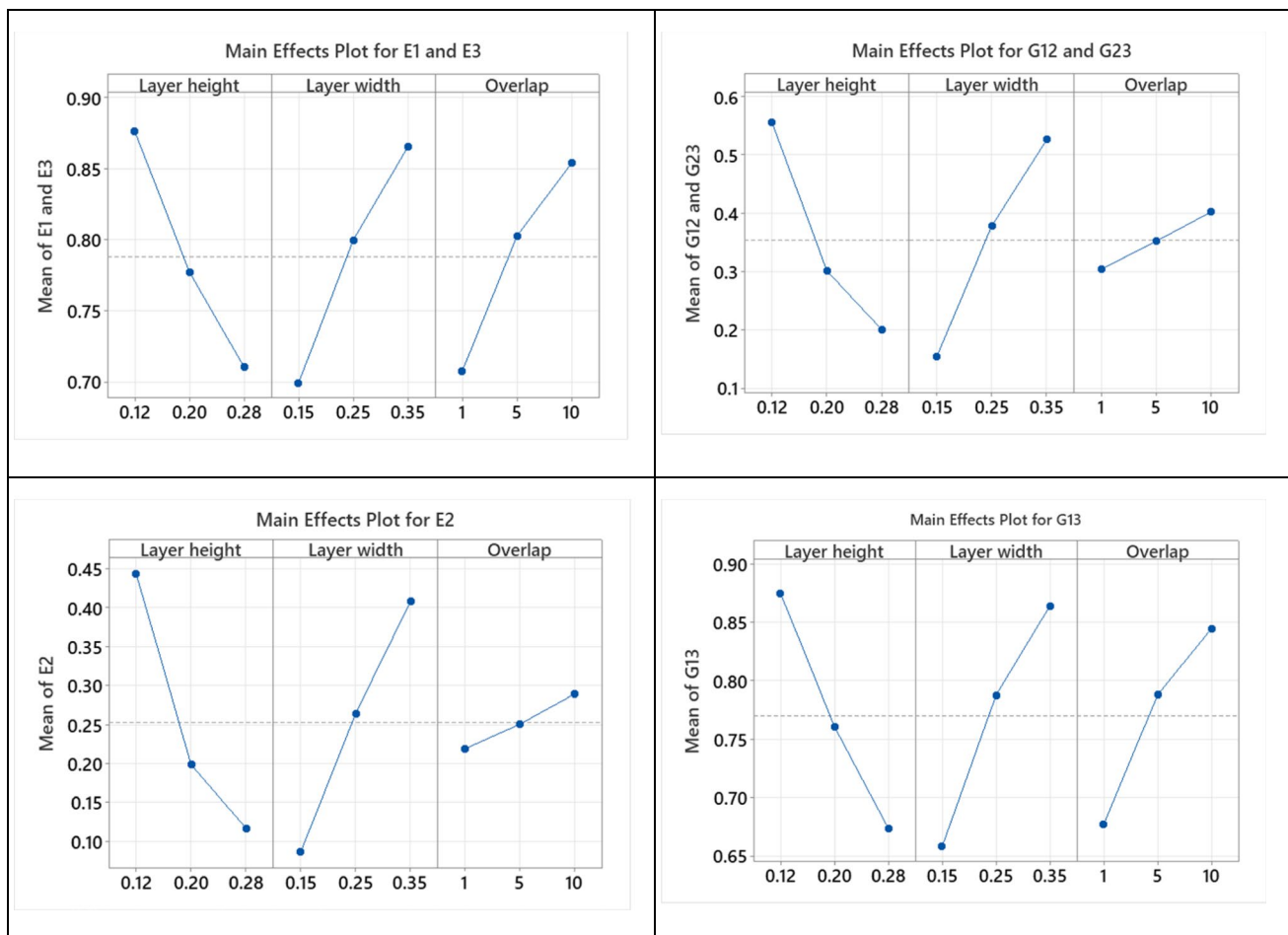


Fig. 8 Main effects plots

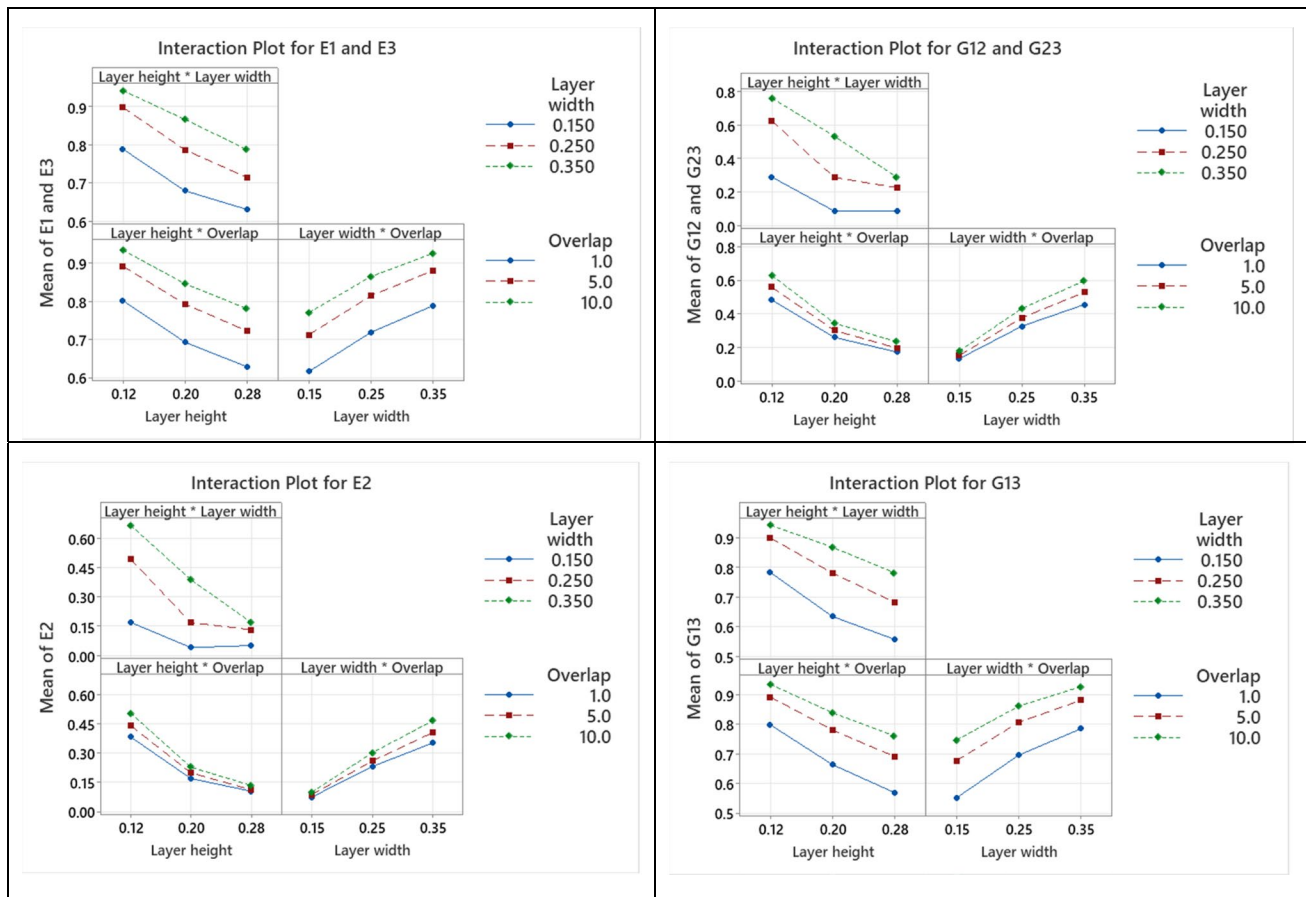


Fig. 9 Interaction effect plots

as well as the interaction effect of layer height/overlapping on the out-of-plane properties of RVE are unlikely.

In summary, analysis of the main and interaction effects from Figs. 8 and 9 reveals that while the size of layer height, layer width and overlapping region affect the in-plane modulus of the RVE (i.e.,  $E_1$ ,  $E_3$  and  $G_{13}$ ) by about  $-14.4\%$ ,  $+14.6\%$  and  $+12.35\%$ , respectively, the layer height, layer width, interaction between layer height/layer width and overlapping region affect the out-of-plane modulus of RVE (i.e.,  $E_2$ ,  $G_{23}$  and  $G_{12}$ ) by  $-12.65\%$ ,  $+12.9\%$ ,  $+4.9\%$  and  $+3\%$ , respectively. This indicates that the layer height can compromise the effect of layer width on both in-plane and the out-of-plane properties of 3D printed parts.

The regression models given in Table 5 were proposed by the full factorial analysis to predict the effective orthotropic properties of the FFF-based 3D printed parts, based on the FE micro-mechanical analysis of RVE. The model was developed by fitting the data in a two-factor interaction model with both significant and insignificant parameters as well as interaction between variables. The positive and negative signs in the equations show the respective positive and antagonistic effects of the variables. The validity

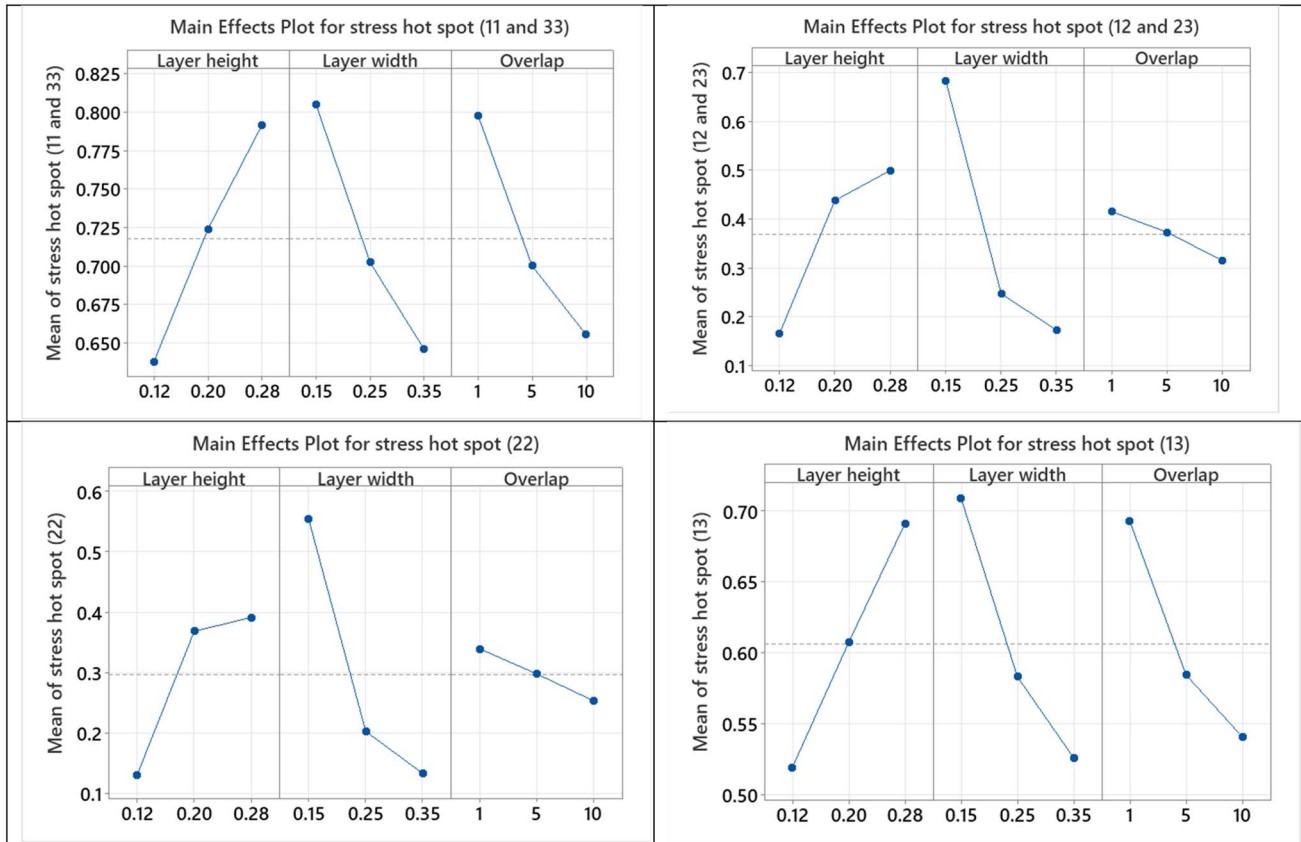
of these models will be discussed in more detail in a case study (Section 4.1).

### 3.4 Influence of layer height, layer width and overlapping on the stress concentration of RVE

The main and interaction effects of variables, i.e., layer height, layer width and overlapping on the mechanical resistance, specifically stress concentration or stress hot spot, of RVEs are illustrated in Figs. 10 and 11. A comparison of these findings with the main and interaction effects of the aforementioned variables on the stiffness properties of RVEs which were detailed in Figs. 8 and 9 reveals the relationship between the stiffness and hot spot stress (i.e., stress concentration) of RVEs in 3D printed materials. These observations indicate that by strategically adjusting various variables to mitigate stress concentration within RVEs, it is possible to enhance the stiffness properties of 3D printed materials. This suggests an inverse relationship between RVE stiffness properties and stress concentration. The main effect depicted in Fig. 10 highlights that while increasing layer

**Table 5** Regression models for the constituents of elastic modulus of RVE. Layer height, layer width and overlapping are denoted as  $A$ ,  $B$  and  $C$ , respectively.  $E$  and  $G$  are Young's modulus and shear modulus of isotropic and homogenous filament materials used for 3D printing

Predicted constituents of elastic moduli	Regression equation	$R^2$ (%)
$E_1 = E_3$	$E \times [0.6773 - 2.137 A + 1.721 B + 0.03217 C + 2.491 A^2 - 1.730 B^2 - 0.001489 C^2 + 0.125 AB + 0.0142 AC - 0.00965 BC]$	99
$E_2$	$E \times [-0.016 - 3.815 A + 4.545 B + 0.0084 \text{Overlap} + 12.68 A^2 - 1.68 B^2 - 0.000020 C^2 - 11.82 AB - 0.0635 AC + 0.0492 BC]$	98
$G_{13}$	$G \times [0.6633 - 2.790 A + 2.103 B + 0.03825 C + 2.074 A^2 - 2.647 B^2 - 0.001810 C^2 + 2.018 AB + 0.0376 AC - 0.02919 BC]$	99
$G_{12} = G_{23}$	$G \times [0.075 - 4.60 A + 5.152 B + 0.0117 C + 11.99 A^2 - 3.78 B^2 - 0.000198 C^2 - 8.42 AB - 0.0588 AC + 0.0524 BC]$	98

**Fig. 10** Main effects plot

width and overlap tends to decrease stress concentration, thereby enhancing the stiffness properties of RVE, elevating the layer height leads to heightened stress concentration, thereby adversely affecting the stiffness properties of RVE. As elaborated in subsequent sections, this phenomenon occurs because an increase in layer height results in larger void sizes, indicating less material across the filament intersections. Consequently, a greater magnitude of localized stress (i.e., stress concentration) at the filament intersections arises across all cases. The analysis of interaction effects among these variables on the stress concentration of RVE, as depicted in Fig. 11, reveals several key findings.

Firstly, compared to the main effects of the variables, the interaction effects between layer height/layer width and layer width/overlap on stress concentration are found to be negligible when RVE is subjected to longitudinal or transverse loading. However, under a shear plane loading scenario of plane 13, the interaction effects among all variables (including layer height/layer width, layer height/overlap and layer width/overlap) become notably pronounced. Furthermore, when RVE experiences loading in shear planes of 12 and 23, the interaction effects between layer height/layer width emerge as significant contributors to RVE stress concentration, surpassing the impact of overlapping. Finally, for the

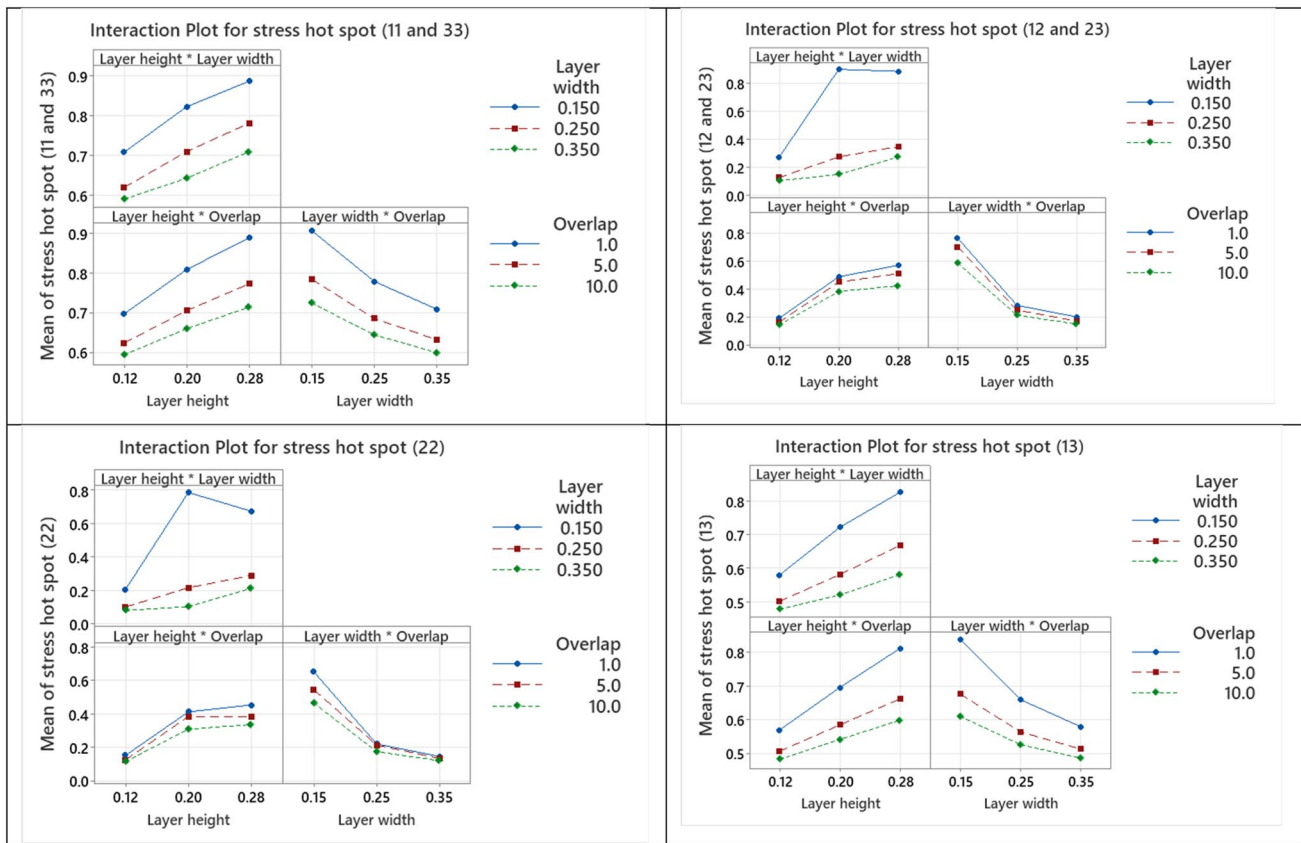
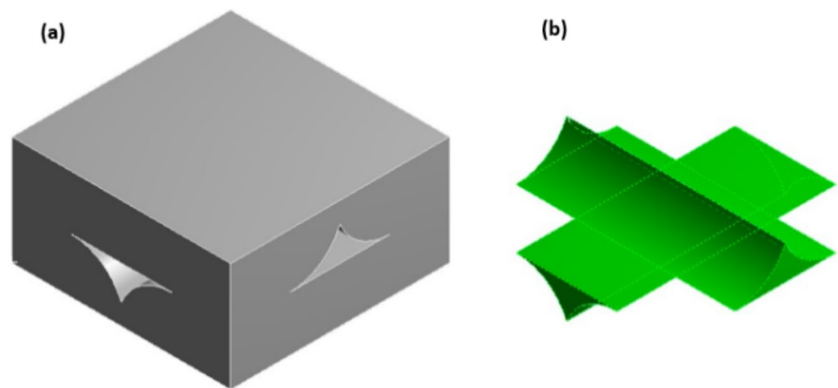


Fig. 11 Interaction effect plots

Fig. 12 a RVE and b schematic view showing the geometry of void inside the RVE



RVE loaded in through the thickness direction, there is a likelihood of interaction effects between layer height/layer width on the stress concentration.

### 3.5 Size effects of inter-bead voids

To determine the void size of all RVEs, the solid micro-model of each RVE, initially constructed in ANSYS Workbench’s design modeller tool, was subsequently imported into the design modeller tool of SOLIDWORKS where

the *mass properties* function was employed to accurately measure the void dimensions. A schematic view of the geometry of void is shown in Fig. 12b. The maximum and minimum values of void size for all trials (27 runs) in design matrix are 27% and 1.18%, respectively. Population characteristics of void size are shown in Fig. 13. It must be noted that these histograms illustrate that the data do not follow a normal distribution. To understand the main effects and interaction effects of variables on the void size, the standard effects plots have been produced in Fig. 14.

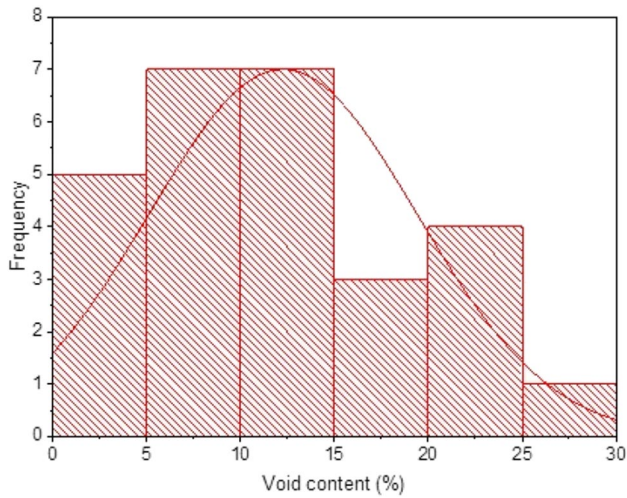


Fig. 13 Histogram of the void size population

As can be seen in this figure, the most important factor affecting the void size is layer width (+17.8%) followed by layer height (-17.4%), overlapping (-9.2) and interaction between layer height and layer width (-2.7%); however, it is unlikely that interaction between layer width and overlap and the interaction between layer height and overlap have a significant impact on the size of void.

The contour plots of void content affected by variables of layer height, layer width and overlapping regions in Fig. 15 indicate that maximizing the layer width and overlapping region and minimizing layer height result in minimizing the size of voids and therefore maximizing the mechanical properties of RVEs of FFF-based 3D printed parts.

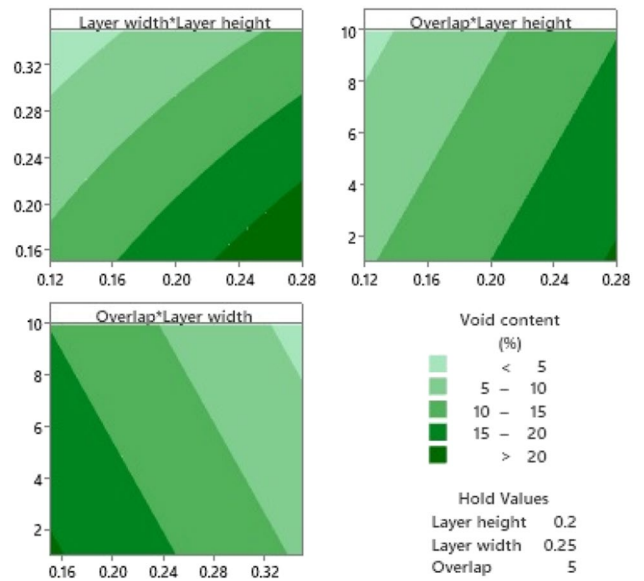


Fig. 15 Contour plots of void content (%)

A regression model given in Table 6 was proposed for the prediction of the void content of the FFF-based 3D printed parts. The model was developed by fitting the data in a two-factor interaction model with both significant and insignificant parameters and interaction between variables (i.e., full quadratic). The positive and negative signs in the equations show the respective positive and antagonistic effects of the variables.

In this study, an exponential equation ( $y = ae^{bx}$ ) was also developed to characterize the effects of void size on the orthotropic properties of RVE where  $a$  and  $b$  are the coefficient and exponent shown in Fig. 16. As it can be seen from the slopes

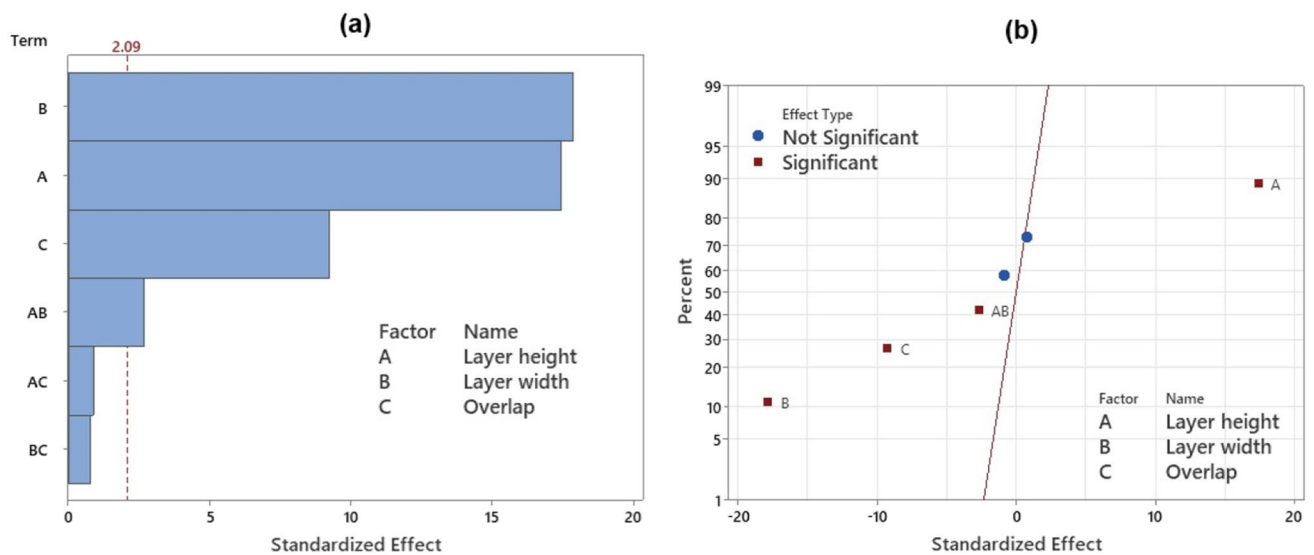
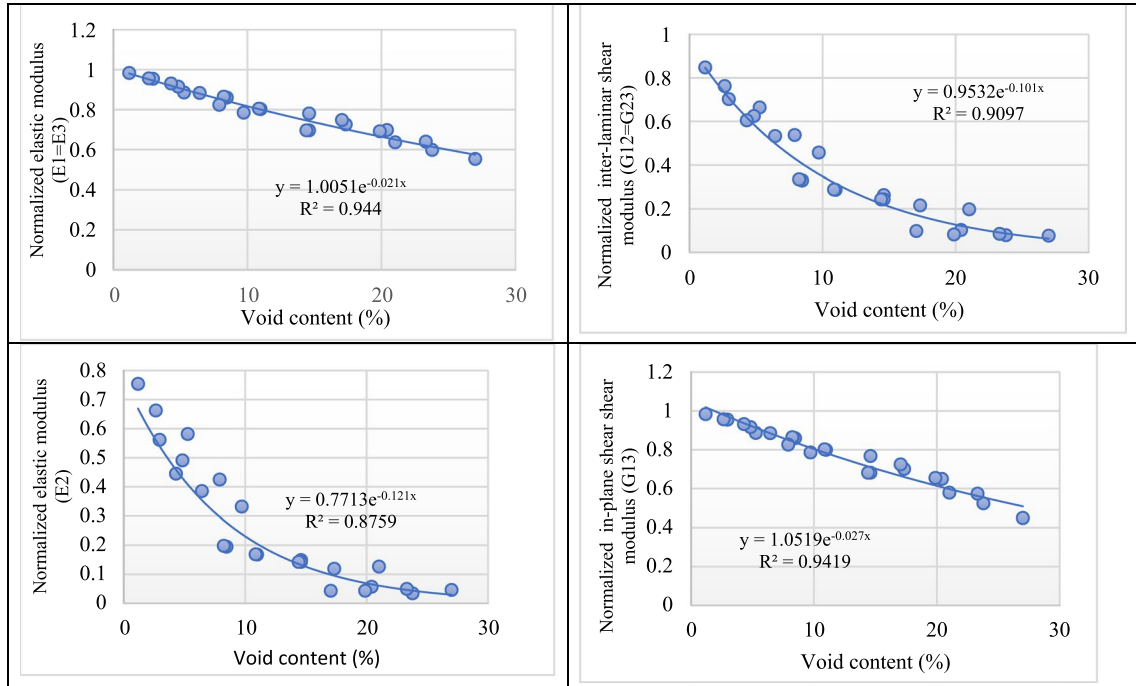


Fig. 14 Plots of the standardized effects (response is void content (%), and confidence level for all intervals is 95%)

**Table 6** Regression models for the prediction of void content of RVE. Layer height, layer width and overlapping are denoted as *A*, *B* and *C*, respectively

Predicted value	Regression equation	$R^2$ (%)
Void content	$12.82 + 156.7A - 98.2B - 1.096 C - 125.4 A^2 + 128.3 B^2 + 0.0423 C^2 - 130.0 AB - 0.0956 AC + 0.0676 BC$	98.5



**Fig. 16** Size effects of void on the elastic properties of RVE of FFF-based 3D printed parts

in this figure, increasing the void size results in reduction of the effective orthotropic properties of the RVE; however, this effect is much more significant on through-thickness and inter-laminar shear properties of the RVE. For example, by increasing the void size from 1.18 to 27%, the longitudinal, transverse and in-plane shear modulus of the RVE reduce by about 45%, but the through-thickness modulus and inter-laminar shear modulus reduce by about 90%. It must be noted that in the methodology for determining reductions in both in-plane and out-of-plane properties of a material filament as a result of void size, 45% and 90% reduction are obtained from these properties based on the original filament properties being considered 100%. The derived values are contingent upon the geometric model assumed for the porous structure. This means that the reductions are calculated relative to the original properties rather than in comparison to the highest value obtained during the analysis process. In essence, this approach ensures that the reductions are standardized based

on the initial properties of the filament rather than being relative to the maximum observed value during analysis.

## 4 Case study

### 4.1 Validation of regression models

In order to validate the regression model developed in this study, a set of layer height, layer width and overlap region which were discussed in Section 3.2 were used in the regression equations detailed in Table 5 to predict the effective orthotropic properties of RVE. The results were then compared to the FE-computed stiffness properties as well as experimentally calculated stiffness properties. As it can be seen in Table 7, the close agreement between predicted FE, experimental and regression model can provide confidence in the use of regression models developed in this study.

**Table 7** Comparison between the stiffness properties of RVE predicted by FEA and regression model for a case study (layer height of 0.2 mm, layer width of 0.3 mm and overlap of 3%)

Response: orthotropic engineering properties		$E_1$ (GPa)	$E_2$ (GPa)	$E_3$ (GPa)	$G_{12}$ (GPa)	$G_{23}$ (GPa)	$G_{13}$ (GPa)
Methodology	<b>FEA homogenization</b>	2.84	0.95	2.84	0.53	0.53	1.05
	<b>Regression model</b>	2.8	0.92	2.8	0.5	0.5	1.03
	<b>Experimental</b>	2.7	0.853	2.7	0.482	0.482	0.952
Difference between regression model and experiments (%)		4	8	4	4	4	8

## 5 Conclusion

In the present investigation, a combined method of numerical homogenization and design of experiment was developed to understand the effect of variables (i.e., layer height, layer width and overlapping region) as well as the effect of void size on the stiffness properties of 3D printed parts. The numerical homogenization technique based on finite element analysis of micro-mechanical models of an RVE was used to predict the influence of the above variables on the elastic response of 3D printed parts (i.e., effective orthotropic properties). To consider the effects of variables on the size of voids, different RVEs were built using design modeller tool of CAD software and subjected to FE homogenization analysis. This is done using a design matrix which was developed by full factorial design of experiment. Some key conclusions are as follows:

- FE analysis of RVE is a useful technique to identify the localized stress at the interfaces between the adjacent filaments/layers and to predict the types of failure modes in FFF-based 3D printed parts. As a result, it is predicted that the potential failure modes in load bearing 3D printed parts where filaments are laid at  $0^\circ$  and  $90^\circ$  are de-bonding between deposited filaments as well as delamination between layers of filament.
- Analysis of the main and interaction effects of variables indicates that the in-plane stiffness properties of the RVE are mainly influenced by layer width, layer height and overlapping region following in importance. However, the out-of-plane stiffness properties of the RVE are further affected by the interaction between layer height and layer width. Despite the negative impact of layer height on the elastic properties of the RVE, layer width, the interaction of layer height/layer width and overlapping region collectively demonstrate a positive influence on the elastic constants.
- Analysis of the main and interaction effects of variables on the size of inter-bead voids indicates that the size of voids is mainly affected by the layer width and layer height, followed by overlapping region and interaction between layer height and layer width. Although the layer

width, overlapping and interaction between layer height and layer width positively affect the stiffness properties of the RVE by minimizing the size of voids, layer height negatively affects the stiffness properties by increasing the void size.

- To optimize the mechanical properties of FFF-based 3D printed parts, the maximum layer width and overlapping regions and minimum layer height are suggested; however, attention must be paid to the cost and time of the manufacturing process as maximizing the layer width and overlapping regions and minimizing the layer height requires more raw filament material to be used in the 3D printing machine.
- The effects of void size on the stiffness properties of RVE indicate that out-of-plane properties of FFF-based 3D printed parts are much more susceptible to variation than in-plane properties. The results of the present investigation show that maximizing the void size will result in reduction of the in-plane and out-of-plane properties of RVE by 45% and 90% respectively. Hence, industrial application of a 3D printed component is significantly limited by the size of inter-bead voids between deposited filaments.
- The exponential equations provided in this study to predict the stiffness properties of RVE for different void contents and also the development of regression models to predict the void size and mechanical properties of FFF-based 3D printed parts based on 3D printing process parameters of layer height, layer width and overlapping regions enable industrial designers and manufacturers to predict the mechanical properties of their final 3D printed products.

The combined numerical and design of experiment method developed in this study showed the ability to predict the elastic properties of 3D printed structures for different 3D printing process parameters of layer width, layer height and overlapping regions. In addition, the size of voids because of these process parameters can be estimated and the size effects of voids on the mechanical properties of 3D printed parts can be predicted. This results in a significant reduction in the number of mechanical tests which are essential to assess the mechanical behaviour of 3D printed parts; as a result, significant time and cost can be saved using

combined FE and DoE approach that has been developed in this study. The approach used in this work also enables designer to conduct faster iterative analysis and choose optimized printing process parameters based on regression models to produce high-quality FFF-based 3D printed parts before time-consuming computational modelling and expensive manufacturing process.

## 6 Future work

While the present study has provided valuable insights into the FE-calculated stiffness properties of RVE when 3D printing process parameters change, it is important to acknowledge the limitations and areas for further investigation. One notable limitation pertains to the assumption concerning boundary conditions, particularly about the choice between planar and non-planar periodic boundary conditions (PBC). In this investigation, a planar PBC was employed due to its existing development in FE software of ANSYS Material Designer. However, it must be noted that a more precise assumption could involve the utilization of non-planar PBC. Moving forward, future research activities could explore the implications of employing non-planar PBC, especially in scenarios where more accurate boundary conditions are crucial for the fidelity of the simulations. However, it is important to acknowledge that modifying this FE-developed software to incorporate non-planar PBC is inherently time-consuming and resource-intensive. Given that the present study is comparative and focused on low porosity cell design, we opted not to invest extensive effort into modifying the current developed FE software, as it falls beyond the scope of our current investigation.

Nevertheless, exploring the effects of different boundary conditions, including non-planar PBC, could enrich our understanding of FE analysis of RVE in 3D printed materials/parts and contribute to the refinement of simulation methodologies in our field. Collaborative efforts within the research community may facilitate the development of tools and techniques that address these challenges. In summary, while the adoption of planar PBC served the objectives of this study, future research could benefit from investigating alternative boundary conditions to enhance the accuracy and applicability of computational models.

## Declarations

**Ethics approval** The work described has not been published before.

**Consent for publication** All authors approved the final manuscript for publication.

**Conflict of interest** The authors declare no competing interests.

**Open Access** This article is licensed under a Creative Commons Attribution 4.0 International License, which permits use, sharing, adaptation, distribution and reproduction in any medium or format, as long as you give appropriate credit to the original author(s) and the source, provide a link to the Creative Commons licence, and indicate if changes were made. The images or other third party material in this article are included in the article's Creative Commons licence, unless indicated otherwise in a credit line to the material. If material is not included in the article's Creative Commons licence and your intended use is not permitted by statutory regulation or exceeds the permitted use, you will need to obtain permission directly from the copyright holder. To view a copy of this licence, visit <http://creativecommons.org/licenses/by/4.0/>.

## References

1. Tao Y et al (2021) A review on voids of 3D printed parts by fused filament fabrication. *J Mater Res Technol* 15:4860–4879
2. Gurralla PK, Regalla SP (2014) Part strength evolution with bonding between filaments in fused deposition modelling: this paper studies how coalescence of filaments contributes to the strength of final FDM part. *Virtual Phys Prototyp* 9(3):141–149
3. Seppala JE et al (2017) Weld formation during material extrusion additive manufacturing. *Soft Matter* 13(38):6761–6769
4. Polychronopoulos ND, Vlachopoulos J (2020) The role of heating and cooling in viscous sintering of pairs of spheres and pairs of cylinders. *Rapid Prototyp J* 26(4):719–726
5. Bhalodi D, Zalavadiya K, Gurralla PK (2019) Influence of temperature on polymer parts manufactured by fused deposition modeling process. *J Brazilian Soc Mech Sci Eng* 41:1–11
6. Huang B, Singamneni S (2015) Raster angle mechanics in fused deposition modelling. *J Compos Mater* 49(3):363–383
7. Tronvoll SA, Welo T, Elverum CW (2018) The effects of voids on structural properties of fused deposition modelled parts: a probabilistic approach. *Int J Adv Manuf Technol* 97:3607–3618
8. Wang X et al (2019) Effect of porosity on mechanical properties of 3D printed polymers: experiments and micromechanical modeling based on X-ray computed tomography analysis. *Polymers* 11(7):1154
9. He Q et al (2020) 3D printed continuous CF/PA6 composites: Effect of microscopic voids on mechanical performance. *Compos Sci Technol* 191:108077
10. Sayah N, Smith DE (2022) Effect of process parameters on void distribution, volume fraction, and sphericity within the bead microstructure of large-area additive manufacturing polymer composites. *Polymers* 14(23):5107
11. Papon EA, Haque A, Mulani SB (2019) Process optimization and stochastic modeling of void contents and mechanical properties in additively manufactured composites. *Compos Part B: Eng* 177:107325
12. Chung S-Y et al (2016) Effects of anisotropic voids on thermal properties of insulating media investigated using 3D printed samples. *Constr Build Mater* 111:529–542
13. Crococolo D, De Agostinis M, Olmi G (2013) Experimental characterization and analytical modelling of the mechanical behaviour of fused deposition processed parts made of ABS-M30. *Comput Mater Sci* 79:506–518
14. Cuan-Urquizo E, Yang S, Bhaskar A (2015) Mechanical characterisation of additively manufactured material having lattice microstructure. *IOP Conference Series: Materials Science and Engineering*. IOP Publishing
15. Garg A, Bhattacharya A (2017) An insight to the failure of FDM parts under tensile loading: finite element analysis and experimental study. *Int J Mech Sci* 120:225–236

16. Gibson L, Ashby M (1999) Cellular solids: structure and properties. Cambridge University Press, Cambridge
17. Hedayati R et al (2017) Analytical relationships for the mechanical properties of additively manufactured porous biomaterials based on octahedral unit cells. *Appl Math Model* 46:408–422
18. Sun C-T, Vaidya RS (1996) Prediction of composite properties from a representative volume element. *Compos Sci Technol* 56(2):171–179
19. Tucker III, C.L. and, Liang E (1999) Stiffness predictions for uni-directional short-fiber composites: review and evaluation. *Compos Sci Technol* 59(5):655–671
20. Guessasma S (2008) Young's modulus of 2D cellular structures under periodic boundary conditions and subject to structural effects. *Comput Mater Sci* 44(2):552–565
21. Liu X, Shapiro V (2016) Homogenization of material properties in additively manufactured structures. *Comput Aided Des* 78:71–82
22. Park S-I et al (2014) Effective mechanical properties of lattice material fabricated by material extrusion additive manufacturing. *Additive Manuf* 1:12–23
23. Domingo-Espin M et al (2015) Mechanical property characterization and simulation of fused deposition modeling polycarbonate parts. *Mater Design* 83:670–677
24. Gonabadi H et al (2022) Investigation of the effect of raster angle, build orientation, and infill density on the elastic response of 3D printed parts using finite element microstructural modeling and homogenization techniques. *Int J Adv Manuf Technol* 1–26
25. Somireddy M, Czekanski A, Singh CV (2018) Development of constitutive material model of 3D printed structure via FDM. *Mater Today Commun* 15:143–152
26. Somireddy M, Czekanski A (2017) Mechanical characterization of additively manufactured parts by FE modeling of mesostructure. *J Manuf Mater Process* 1(2):18
27. Shergill K, Chen Y, Bull S (2023) An investigation into the layer thickness effect on the mechanical properties of additively manufactured polymers: PLA and ABS. *Int J Adv Manuf Technol* 126(7–8):3651–3665
28. Vardhan Rai H, Kumar Modi Y, Pare A (2018) Process parameter optimization for tensile strength of 3D printed parts using response surface methodology. *IOP conference series: materials science and engineering*. IOP Publishing
29. Gonabadi H et al (2022) Investigation of the effect of raster angle, build orientation, and infill density on the elastic response of 3D printed parts using finite element microstructural modeling and homogenization techniques. *Int J Adv Manuf Technol* 118(5):1485–1510
30. Gonabadi H et al (2021) Investigation of anisotropy effects in glass fibre reinforced polymer composites on tensile and shear properties using full field strain measurement and finite element multi-scale techniques. *J Compos Mater* 00219983211054232

**Publisher's Note** Springer Nature remains neutral with regard to jurisdictional claims in published maps and institutional affiliations.